Joint Shear Deformation and Beam Rotation in RC Beam-Column Eccentric Connections

Rooh Ullah [1*], Muhammad Fahim [2], Muhammad Nouman [2]

[1] MS Structural Engineering Student, University of Engineering and Technology Peshawar, KPK, Pakistan.

[2] Faculty Member, University of Engineering & Technology Peshawar, KPK, Pakistan.

Abstract

This paper discusses joint shear deformation and beam rotation for RC beam-column eccentric connections. Two eccentric connections were designed according to ACI 318-14 and ACI-352 and their half scaled models were constructed sequentially to introduce a cold joint at the beam column interface. Specimen having eccentricity equal to $bc/8$ (12.5% of column width) and $bc/4$ (25% of column width) were named as specimen 1 and specimen 2 respectively. The specimens were tested under quasi static full cyclic loading. The results are presented in the form of beam rotation versus drift and beam rotation versus lateral load plots. In addition, joint shear deformation versus drift is also plotted for both specimens. Careful observation of the damage pattern revealed that bond slip occurred at 2.5% drift in both specimens with no yielding of beam longitudinal bars in the joint core due to the presence of construction joint. An increase in out of plane rotation was observed with increase in eccentricity. However, in plane rotation was more in specimen 1 as compared to specimen 2, primarily due to negligible out of plane rotations. Furthermore, joint shear deformation increased with increase in eccentricity. However, it was negligible due to slab contribution as well as bond slippage with minimum load transfer to the joint core. It is concluded that bond slippage is the principal failure pattern whereas out of plan rotation increases with eccentricity without significant contribution to the final failure pattern.

Keywords: Eccentricity; Beam-column Connection; Cold Joint; Joint Shear Deformation; Beam Rotation.

1. Introduction

Beam-column connection is a very critical region in reinforced concrete structures to transfer forces, particularly when subjected to earthquake loading. In order to dissipate high energy and to avoid overall strength degradation, beam hinging is the desirable mode of failure, while avoiding column hinging and joint shear deformation. There are two types of connections defined in ACI-352R-02 [1], called type 1 and type 2 connection. Type 1 connection are those which are designed for gravity loads and not for significant inelastic deformation. Similarly, type 2 connection are designed to withstand strength under deformation reversal into inelastic range [1]. Since mid-1960's beam-column connections in reinforced concrete has been an active area of experimental studies. Various parameters have been investigated in beam-column connections and the effect of these parameters were integrated in ACI 352R-02 document [2]. This paper presents joint shear deformation and beam rotation for reinforced concrete (RC) beam-column eccentric connections. Response of beam-column connections varies unfavourably when there is eccentricity between beam and column centrelines called horizontal eccentricity and eccentricity between beam-beam centrelines

---

called vertical eccentricity [3-7]. Similarly, axial force on a column, poor detailing in connections, beam-wide column joint, anchorage methods, connections with slab etc. have very significant effect on dynamic characteristics of beam-column connections [8-11]. As horizontal eccentricity is one of the architectural requirements in reinforced concrete structures, so it is important to investigate the negative influence of horizontal eccentricity on the dynamic characteristics of beam-column connections [12]. In connections, joint shear demand occurs because of beam longitudinal bars plus slab longitudinal bars within the effective width of slab [1].

When there is horizontal eccentricity between beam and column centrelines, the resultant of these forces concentrates towards flush side of beam resulting in torsion demand in the joint region which produces extra demand on the joint [2, 12]. This extra demand is responsible for reducing shear strength of joints, varying damage pattern of connections, reducing displacement ductility and energy dissipation of connections, overall force-deformation behaviour of connections, etc. [2, 12]. The joint shear deformation has been found to be approximately 4 to 5 times on flush side as compared to offset side of a beam [12]. Similarly joint shear deformation reduces somehow by including slab in eccentric beam-column connections due to shifting of the force resultant by slab longitudinal bars [2, 13]. In addition, beam rotation also occurs in eccentric connections due to torsional effect induced by eccentricity [12]. However, by including slab in beam-column connections torsional effect reduces in eccentric connections [2, 13]. The joint shear deformation has been found to be negligible up to 1% drift in eccentric connections as compared to concentric connection. However, the joint shear deformation increases significantly as eccentricity increases. Similarly the joint shear deformation was also significantly influenced by degree of damage at beam column interface [16]. In addition when the eccentricity reached to bc/4 the ductile mode of failure changes to brittle mode of failure [17]. The effect of closing and opening was observed significantly in eccentric connection due to torsional forces [18]. Many studies have investigated the eccentricity effect on beam-column connections without slab and very few researchers have included slab as part of the eccentric beam-column connections in their investigation. However, they only considered eccentric connections of exterior frames. In this study eccentric corner connections with slab were investigated for joint shear deformation and beam rotation having construction joint just above and below the beam longitudinal bars in joint core.

The following section briefly discusses methodology of the study which includes specimen designing, scaling of specimens, material testing, construction of specimens, test setup, and instrumentation. This is followed by results and discussions which include damage pattern at different drift levels, in-plane beam rotations and joint shear deformations. Conclusions drawn are discussed in the end.

2. Research Methodology

The step by step process followed in the research program is shown in the flowchart shown in Figure 1. The steps shown are discussed in the subsequent sub sections.
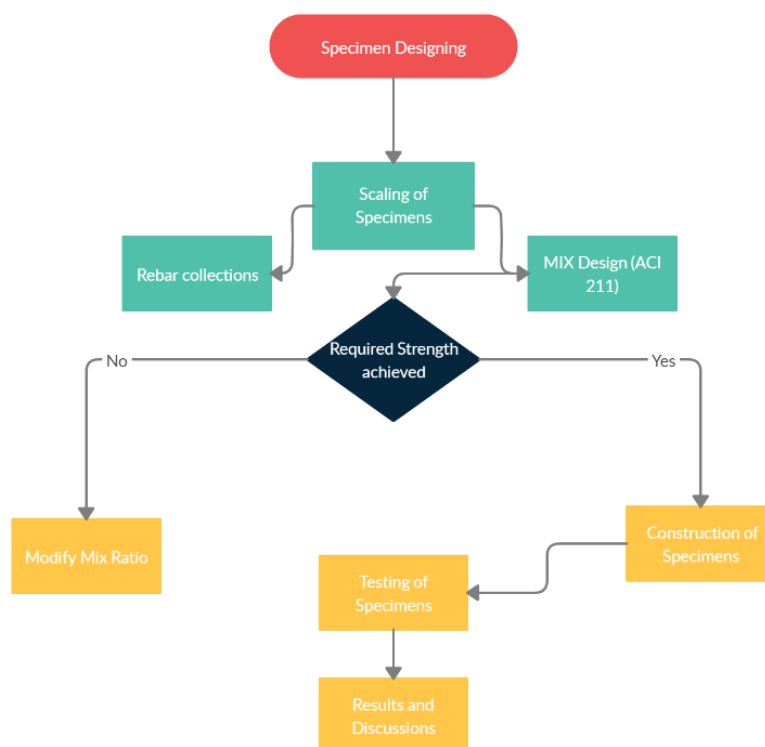

Figure 1. Step by step process followed in the study

2.1. Designing and Scaling of Specimens

A total of two specimens were designed according to ACI 318-14 [14] and ACI 352R-02 [1]. These were named as specimen 1 and specimen 2 with horizontal eccentricities of bc/8 (12.5% of column width) and bc/4 (25% of column width) respectively. The eccentricity effect has been neglected in ACI 352R-02 [1] up-to bc/8 (12.5% of column width).
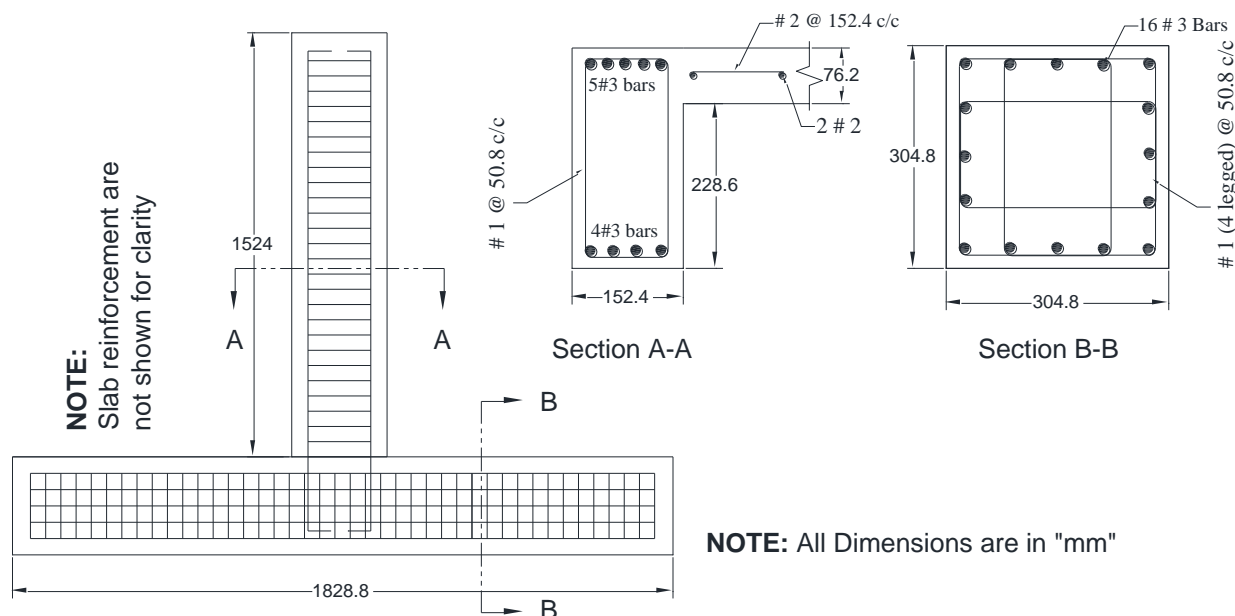

Figure 2. Reinforcement details of scaled specimens

The reinforcement details were identical in the two specimens as shown in Figure 2. Column was reinforced with 16 # 6 bars ($\rho = 1.22\%$), while reinforcement in spandrel beam was 5 # 6 bars ($\rho = 0.76\%$) in top layer and 4 # 6 bars ($\rho = 0.61\%$) in bottom layer. Similarly, the reinforcement in normal beam was 3 # 6 bars in top layer and 2 # 6 bars in bottom layer. In slab, #4 bar @ 152.4 mm (6 inch) centre-to-centre spacing for transverse reinforcement has been used, while 2 # 4 bars were used in longitudinal direction. For comparison, researchers have used $\rho = 1.5\%$, $\rho = 0.79\%$, and $\rho = 0.39\%$ for column, spandrel beam top and bottom layers respectively [2].

Both specimens were identical except the location of spandrel beam (eccentricity between beam and column centerline). The spandrel and normal beams were 304.8 mm (12 inch) wide and 609.6 mm (24 inch) deep, and span of spandrel beam was 609.6 mm (240 inch) in prototype. Similarly, the length of normal beam was kept equal to the effective width of floor slab. The column was 609.6 mm (24 inch) wide and 609.6 mm (24 inch) deep in order to provide enough space for the required eccentricity by changing beam location. The prototype story height was taken 3657.6 mm (144 inch). The thickness of slab was 152.4 mm (6 inch) and its width is equal to the effective width recommended by ACI 318-14 (section 8.4.1.8).

Both specimens were then scaled down keeping in view the availability of facilities in structural laboratory at Civil Engineering Department of University of Engineering and Technology, Peshawar, Pakistan. Half scale was selected and specimens were scaled down by using dimensional analysis and Buckingham Pi Theorem for static case. The stress σ, strain ε, and Poisson's ratio υ, for materials were kept identical to prototype materials.

2.2. Material Testing

Load versus displacement graphs for both concrete and steel were drawn after testing concrete cylinders and steel samples as shown in Figures 3 and 4 respectively. During construction, at least three cylinders were cast for each pouring stage and were tested for concrete compressive strength. Similarly, three samples of steel bars were tested for different sizes of steel used in specimens. The average compressive strength of concrete cylinders at specimens testing time was 4,200 psi and yield strength of steel was 65,000 psi.
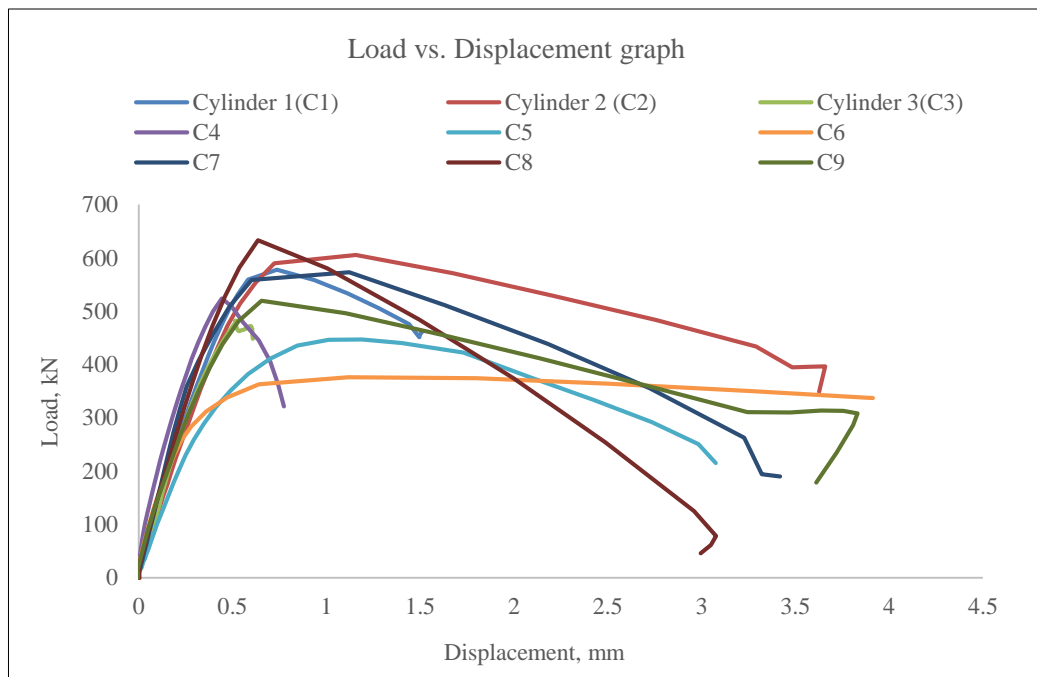
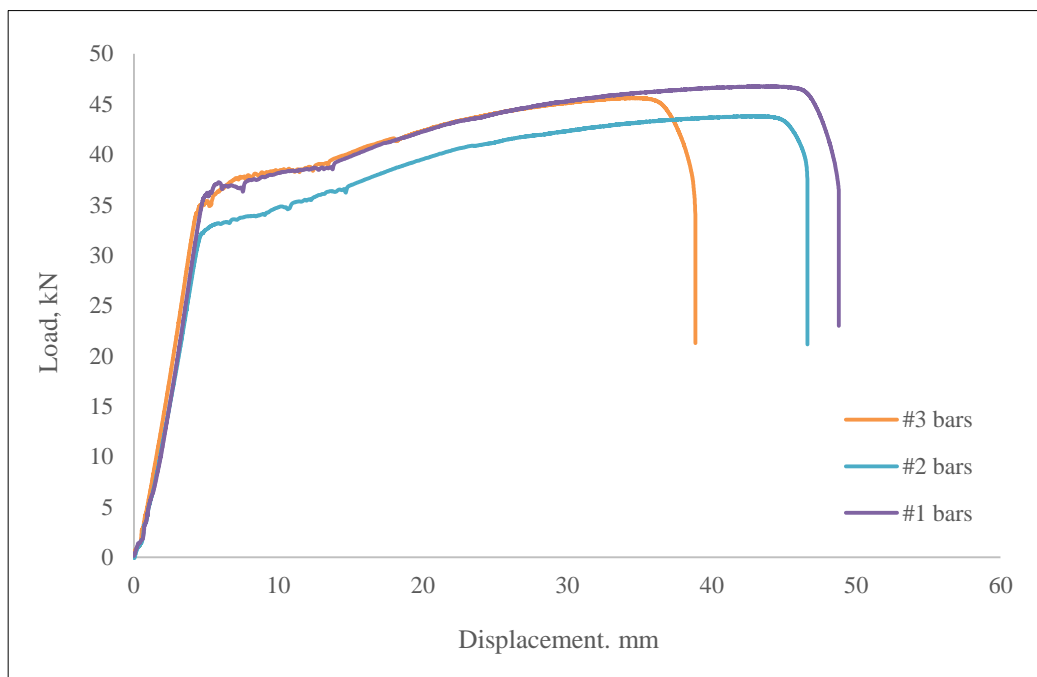**Figure 3. Load vs. displacement graph of nine concrete cylinders**

Figure 4. Load vs. displacement graph for different sizes of steel bars used in specimens

2.3. Construction of Specimens

Construction of specimens includes preparation of steel cages, welding of steel plates at top and bottom column for anchorage, installation of strain gauges at critical locations, preparation of formwork, and casting of specimens as shown in Figure 5.

Both specimens were cast by laying column horizontally and beam along with slab vertically. Sequential pouring was done during casting of both specimens to study the cold joint effect. At first, top and bottom columns were poured at the same time followed by pouring of joint, beam and slab after 7 days as shown in Figure 5. This sequential casting developed construction joint just above and below the beam longitudinal bars for both top and bottom layers in the joint core.
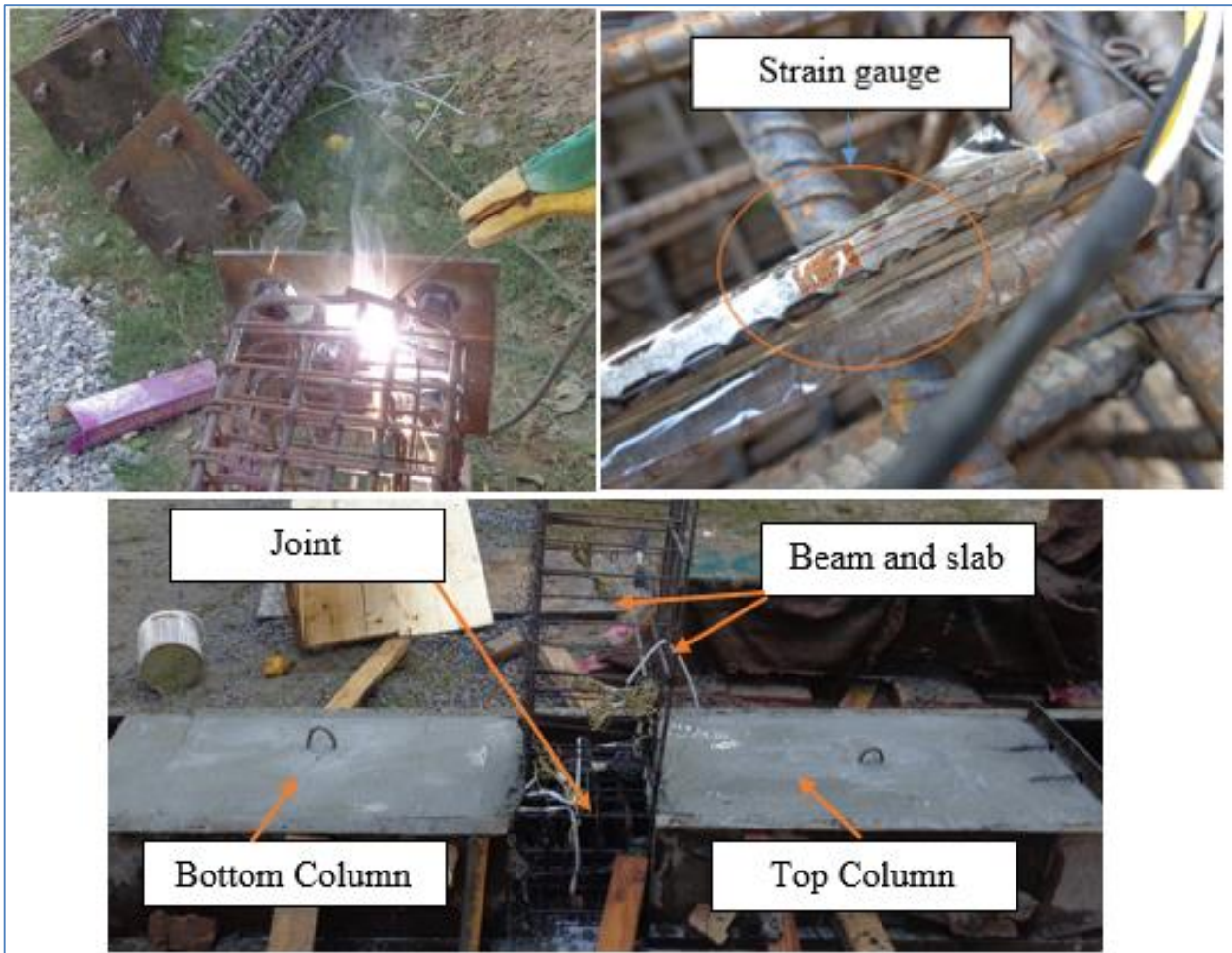
Figure 5. Steel plate welding, strain gauge installations, and sequential pouring

2.4. Test Setup and Instrumentations

The test setup as depicted in Figure 6, was based on assumptions that the point of contra-flexure occurs at middle points of both top and bottom columns. Due to this assumption, bottom column was connected directly to pin connection while top column end was horizontally restrained only, thus allowing vertical displacement as well as moment if any. Similarly, beam tip was connected to the universal hinge to allow rotation of beam as expected in eccentric connection.

Axial load of 32 ton (3.45 MPa) was applied on top column and retained till the end of test. Full reverse cyclic loading was applied on the beam tip as shown in Figure 7. Similarly, for beam rotation, a total of four linear variable displacement transducers (LVDT) named LVDT 5, 6, 7, and 8 were installed at beam-column interface. In addition to this, two dial gauges named dial gauge 3 and 4 were installed diagonally at flush side of beam to measure joint shear deformation as shown in Figure 8.
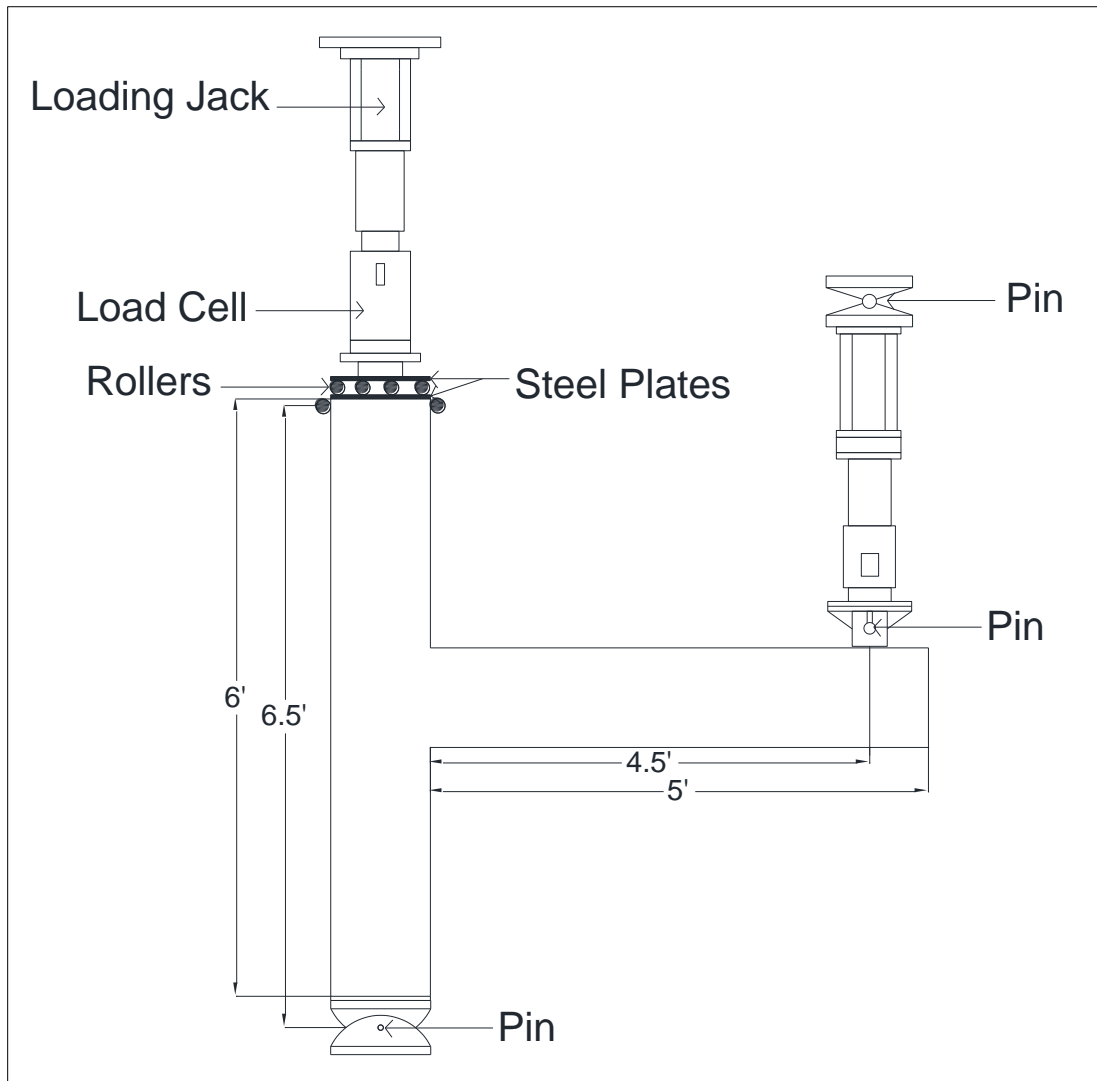
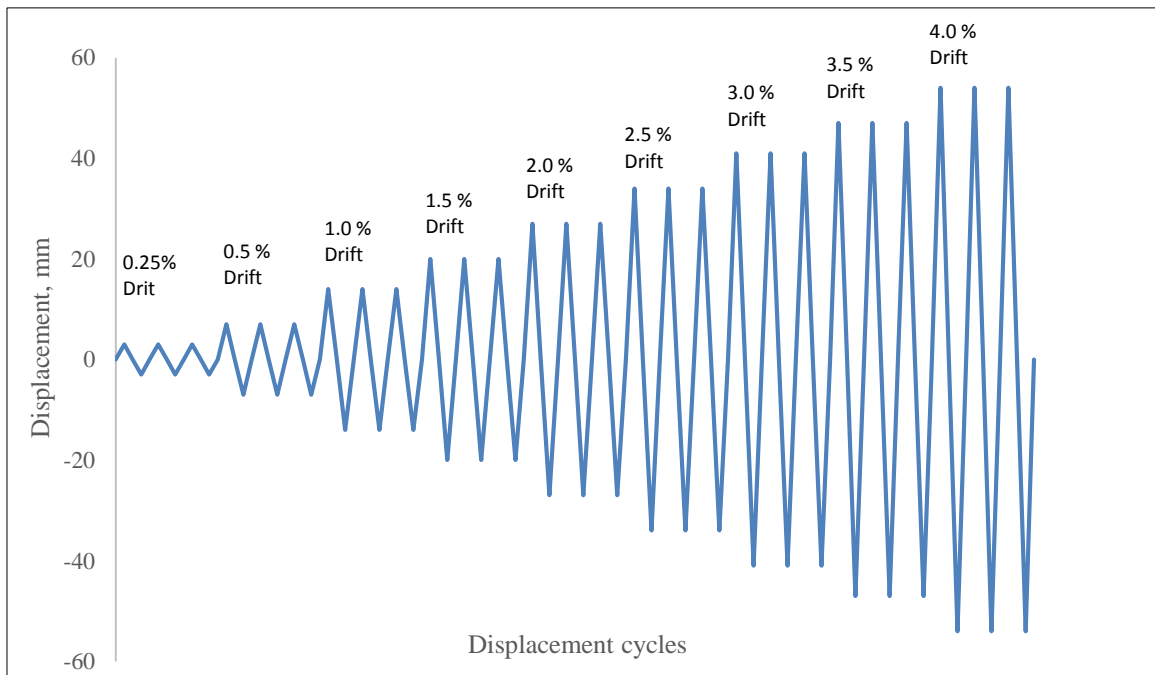**Figure 6. Boundary conditions and loading setup**

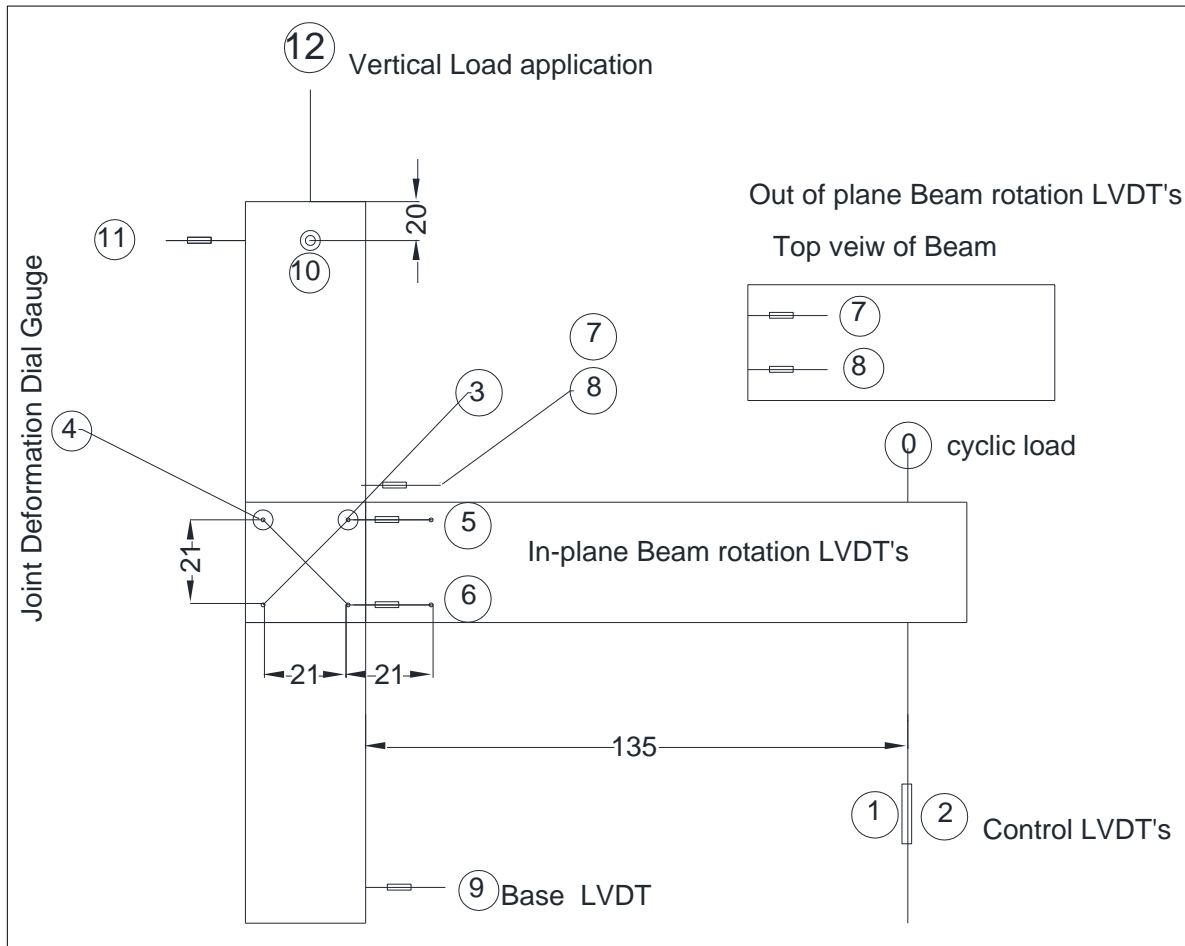**Figure 7. Displacement history for both specimens**

Figure 8. Instrumentation details for both specimens (All dimensions are in centimeters, cm)

3. Results and Discussions

There are many factors which contribute to beam tip displacements and rotations like joint shear deformation, bond slip in joint region, yielding penetration to joint regions and plastic hinge formation as shown in Figure 9. Similarly, other elastic components like shear and flexural deformation in beam and column also have some contributions to beam tip displacements but negligible [15].
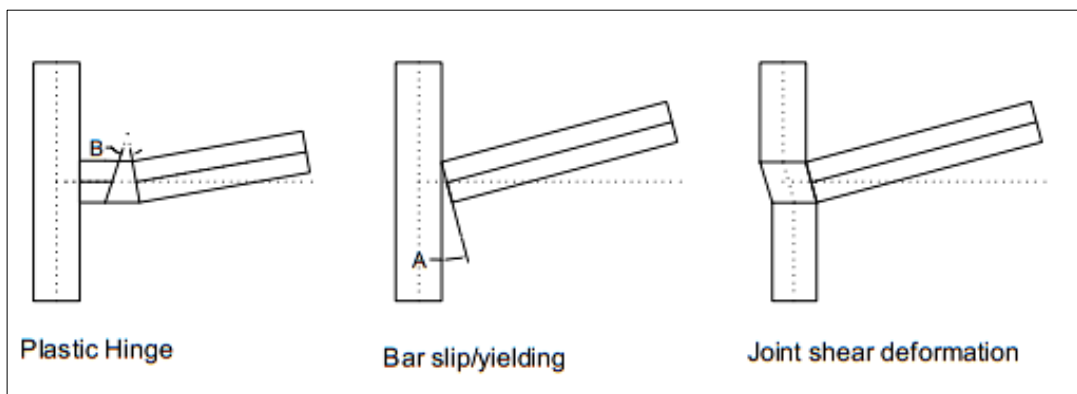

Figure 9. Main factors that contributes to beam tip displacements

3.1. Damage Mechanism of Both Specimens

3.1.1. Damage Pattern at 1% Drift

The inception of hairline cracks started at 1% drift. It can be seen in Figure 10 that the cracks appeared in the vicinity of beam-column interface in both specimens.

Figure 10. Crack pattern of specimen 1 (bc/8) and specimen 2 (bc/4) at 1% drift

3.1.2. Damage Pattern at 1.5% Drift

At 1.5% drift, further crack distribution was observed on both exterior and interior face of specimens as shown in Figure 11, showing excellent energy dissipation. Similarly, in specimen 1 widening of cracks was seen at beam-column interface. However, no such widening was observed in specimen 2.
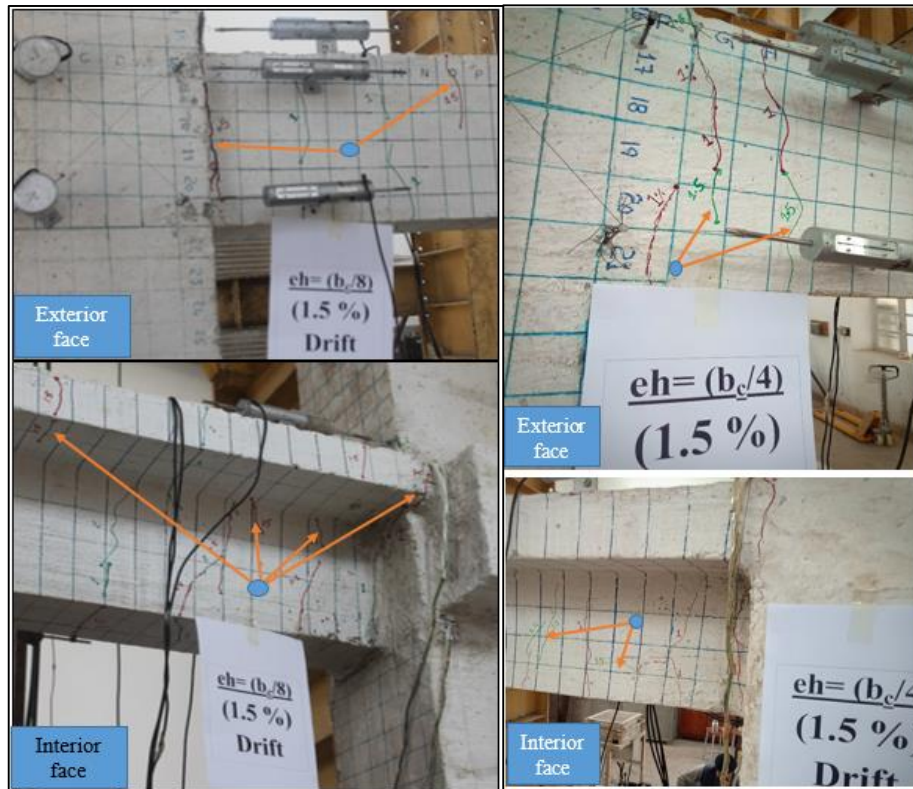

Figure 11. Crack pattern of specimen 1 (bc/8) and specimen 2 (bc/4) at 1.5% drift

3.1.3. Final Damage Pattern

At 2% drift the cracks started widening in both specimens at beam-column interface with additional minor crack distributions as depicted in Figure 12. Final crack pattern shows similar trend to bar slip/yielding case as discussed in Figure 9. The yield strain of steel bars used in both specimens was 0.0125. Similarly, the strain gauges show a maximum strain of 921E-6 (0.000921) at 1.5% drift. After 1.5% drift, all strain gauges got damaged. In addition, the hook bar development length was provided more than that proposed by section 4.5.2.4 of ACI 352R-02. Based on this it is concluded that pull-out phenomena occurred at beam-column interface. This is primarily due to sequential construction of both specimens.
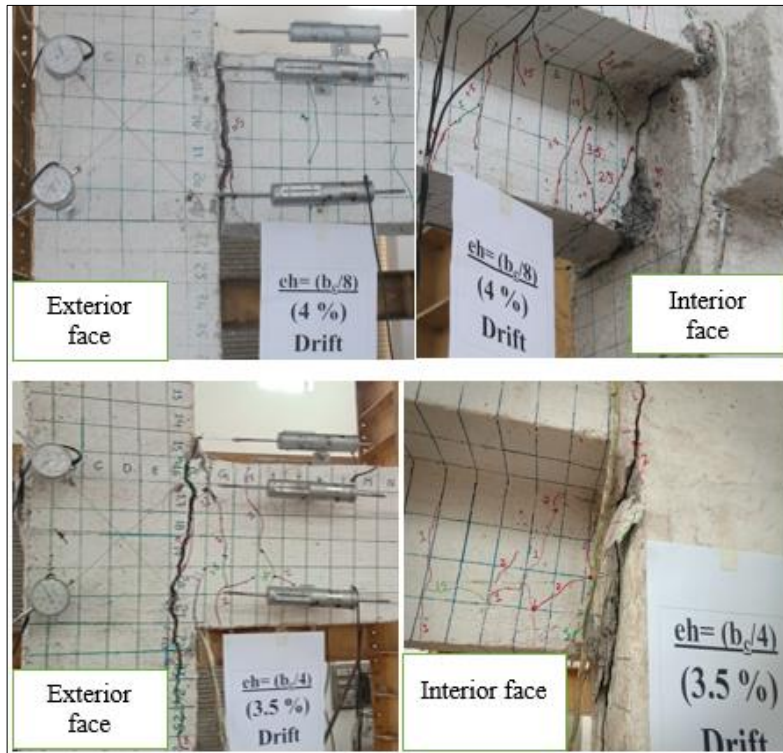

Figure 12. Final damage pattern of specimen 1 (bc/8) and specimen 2 (bc/4)

3.2. In-plane Beam Rotation

All LVDTs had a range of 50 mm (25mm in either direction). The data from LVDT 7 and 8 was ignored due to exceeding limit of 25 mm. Thus only LVDT 5 and 6 were analyzed for both specimens.

All the readings of LVDTs were plotted against beam tip displacement and the eccentricity effect of both the specimens were compared. Beam's in-plane rotation at both LVDTs was calculated using Equation 1. A sample of beam in-plane rotation is shown in Figure 13. The total depth of beam was 12 inch (304.8 mm) in both scaled models. The center to center distance between LVDT 5 (beam top) and 6 (beam bottom) was kept 8.27 inch (210 mm) as depicted in Figure 8.

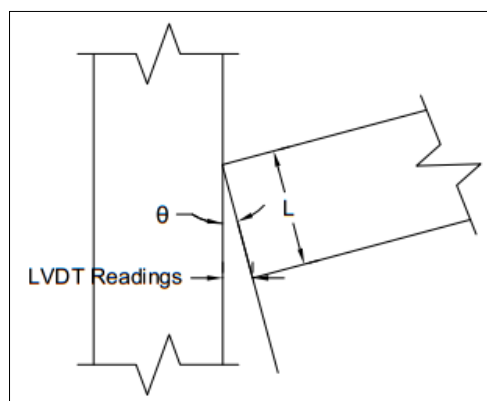$$\theta = \tan^{-1}(\frac{perp}{base}) \tag{1}$$

Figure 13. In-plane beam rotation

3.2.1. Beam Top Displacement at Beam-column Interface

Beam top displacement at beam-column interface was recorded using LVDT 5. As shown in Figures 14 and 15, LVDT 5 shows similar trend for both specimen 1 and 2. Specimen 1 showed negligible displacement in positive cycles as compared to specimen 2. However, in negative cycle's specimen 1 showed 16.5 mm displacement and specimen 2 showed 9.3 mm displacement at 47 mm (3.5 % drift) beam tip displacement. By using Equation 1, specimen 1 and specimen 2 experienced 0.172 radians and 0.1 radians beam rotations with respect to beam column interface, respectively.
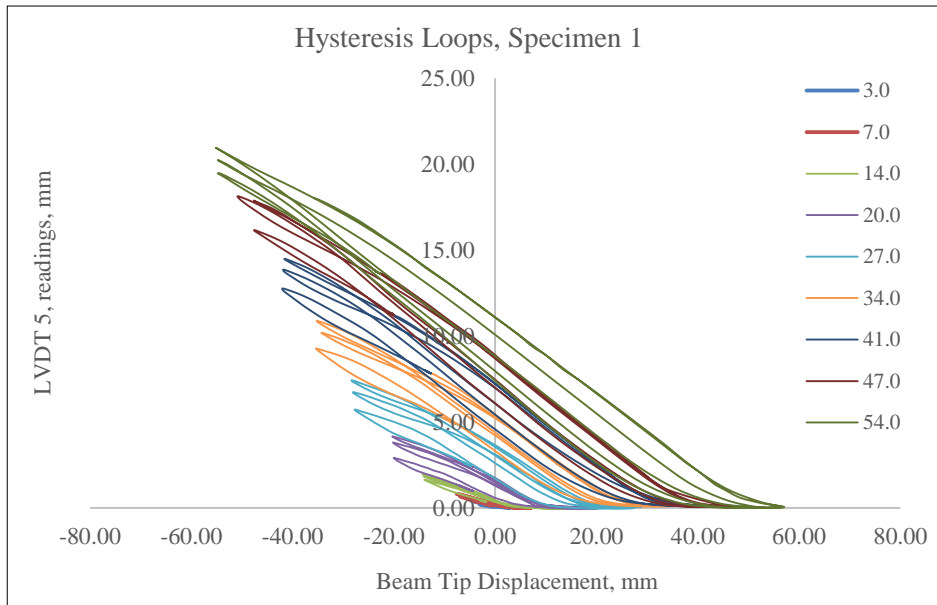

Figure 14. Beam top displacement at beam-column interface vs. beam tip displacement for specimen 1
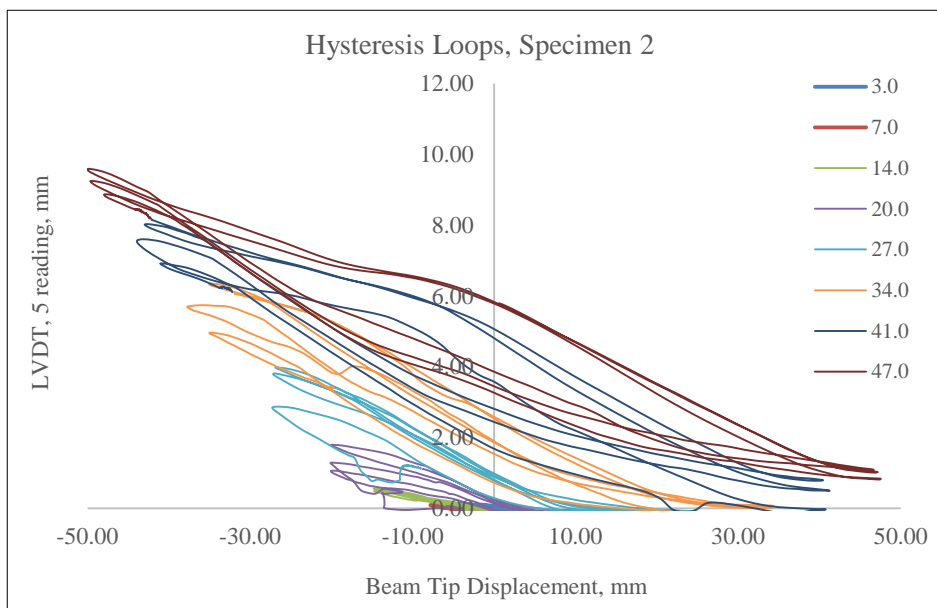

Figure 15. Beam top displacement at beam-column interface vs. Beam tip displacement for specimen 2

3.2.2. Beam Bottom Displacement at Beam-column Interface

Displacement at beam bottom face near beam-column interface was recorded using LVDT6. LVDT 6 readings versus beam tip displacement for both specimens are shown in Figures 16 and 17 respectively. At 47 mm (3.5% drift) beam tip displacement, specimens 1 and 2 experienced 6.5 mm and 3.82 mm displacement respectively in positive displacement cycles. Similarly in negative displacement cycles at 3.5 % drift, specimen 1 experienced 12.5 mm displacement and specimen 2 experienced 0.9 mm displacement. By using Equation 1, specimen 1 and specimen 2 developed a maximum of 0.07 radians and 0.04 radians beam rotations respectively with respect to beam column interface.
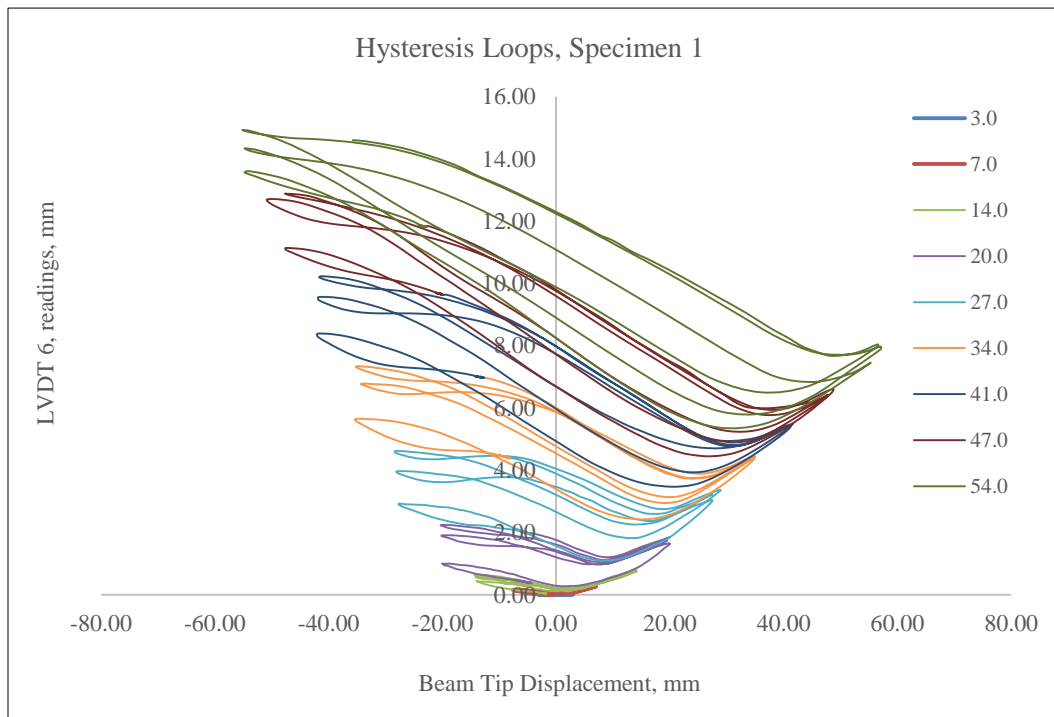
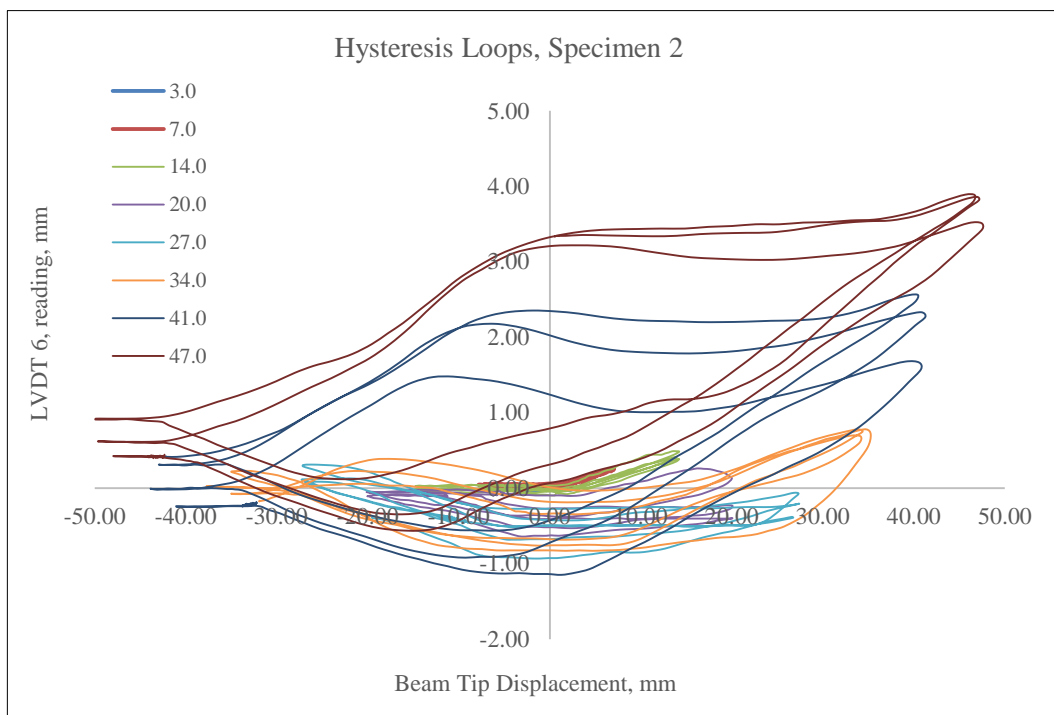**Figure 16. Beam bottom displacement at beam-column interface vs. Beam tip displacement for specimen 1**

Figure 17. Beam bottom displacement at beam-column interface vs. Beam tip displacement for specimen 2

3.2.3. Comparison of LVDT 5 (Beam Top) and LVDT 6 (Beam Bottom)

LVDT 5 and LVDT 6 for both specimens are compared in Figure 18. The in plane rotation of specimen 1 was more than specimen 2, this is due to out of plan rotation in specimen 2 beam due to high eccentricity. LVDT 7 and 8 were used for recording out of plan rotation of beam. In specimen 2, out of plan rotation was beyond the LVDT limit (25 mm in either direction). Similarly, by comparing LVDT 5 and LVDT 6 of same specimen, it can be seen that LVDT 5 shows more in plane rotation than LVDT 6. This is primarily due to more torsional rotation at beam bottom face as compared to beam top face. Beam top surface shows less torsional rotation as compared to beam's bottom surface, because the slab part stiffened the beam-top surface.
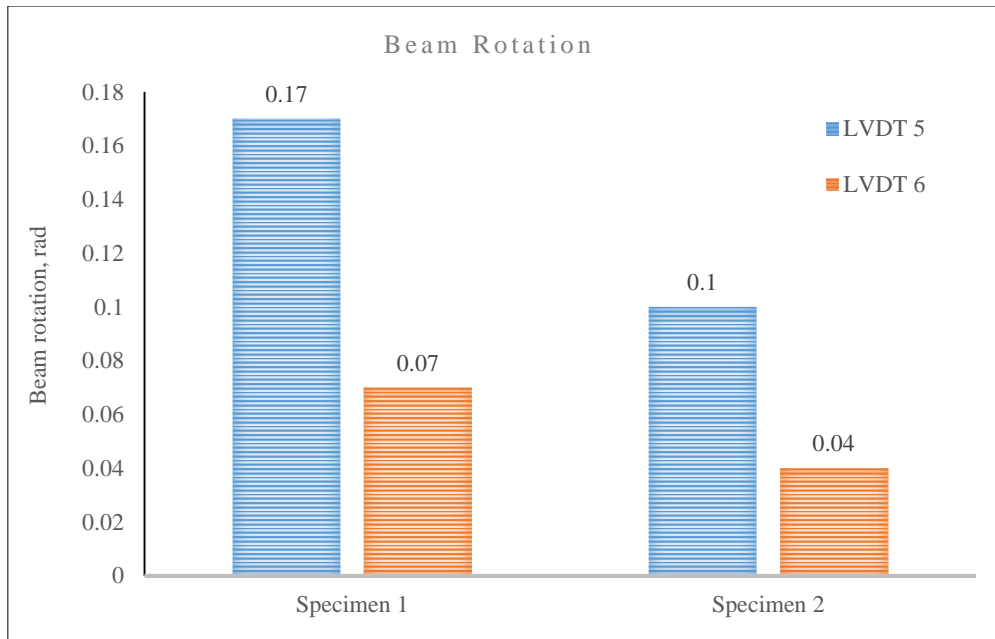
Figure 18. Comparison of beam rotation for both specimens

3.2.4. Beam Top Displacement at Beam-column Interface versus Lateral Load

LVDT 5 readings versus lateral load are shown in Figures 19 and 20 for specimen 1 and specimen 2 respectively. At 3.5 % drift, specimen 1 experienced 16.1 mm displacement and the corresponding load was 15.5 KN, while specimen 2 experienced 9.3 mm displacement with corresponding load of 8.8 KN.
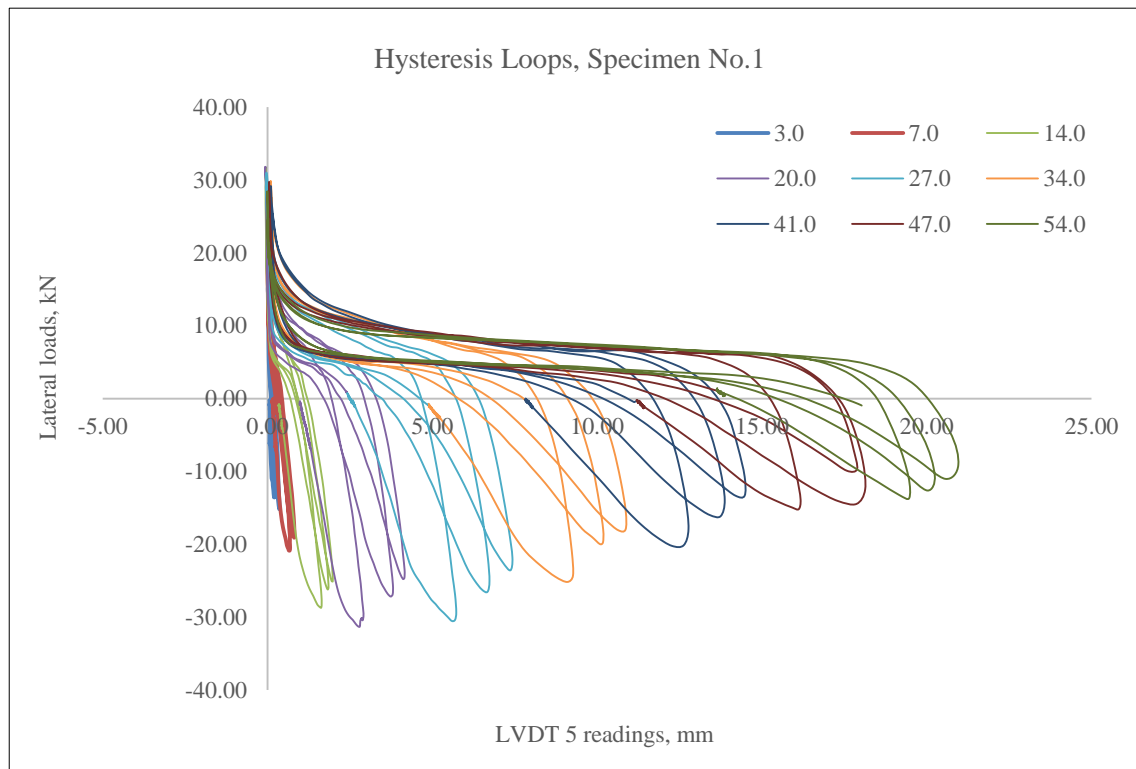

Figure 19. Beam Top displacement at beam-column interface vs. Lateral loads, Specimen 1
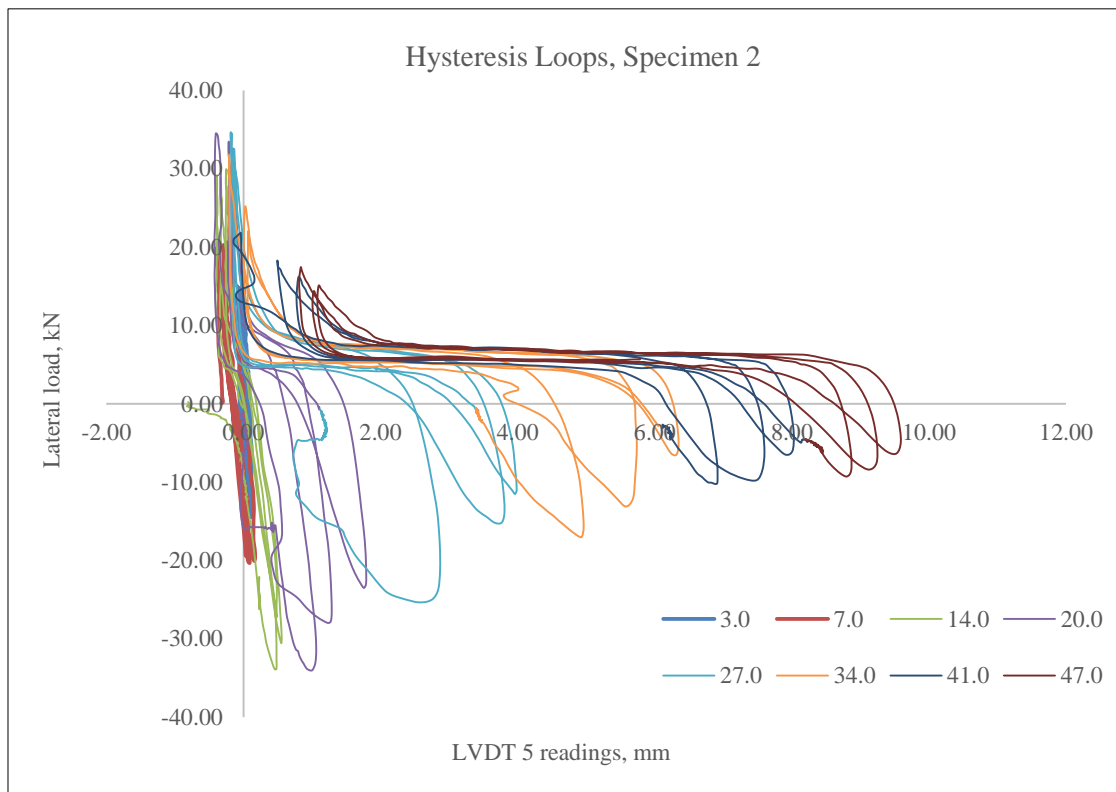
Figure 20. Beam bottom displacement at beam-column interface vs. Lateral loads, Specimen 2

3.2.5. Beam Bottom Displacement at Beam-column Interface versus Lateral Load

The readings of LVDT 6 versus lateral load are shown in Figures 21 and 22 for specimen 1 and 2 respectively. Due to greater torsional effect in specimen 2 the hysteresis loop of specimen 2 was not meaningful as compared to specimen 1.
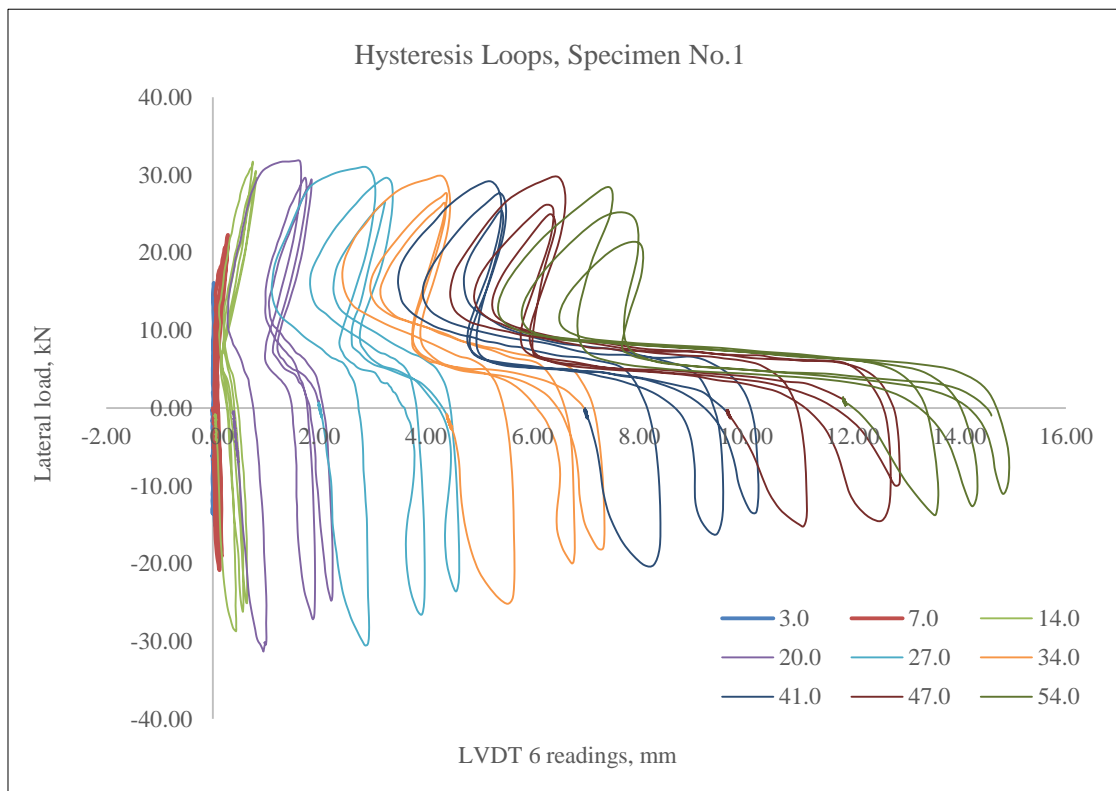

Figure 21. Beam bottom displacement at beam-column interface vs. lateral loads, Specimen 1
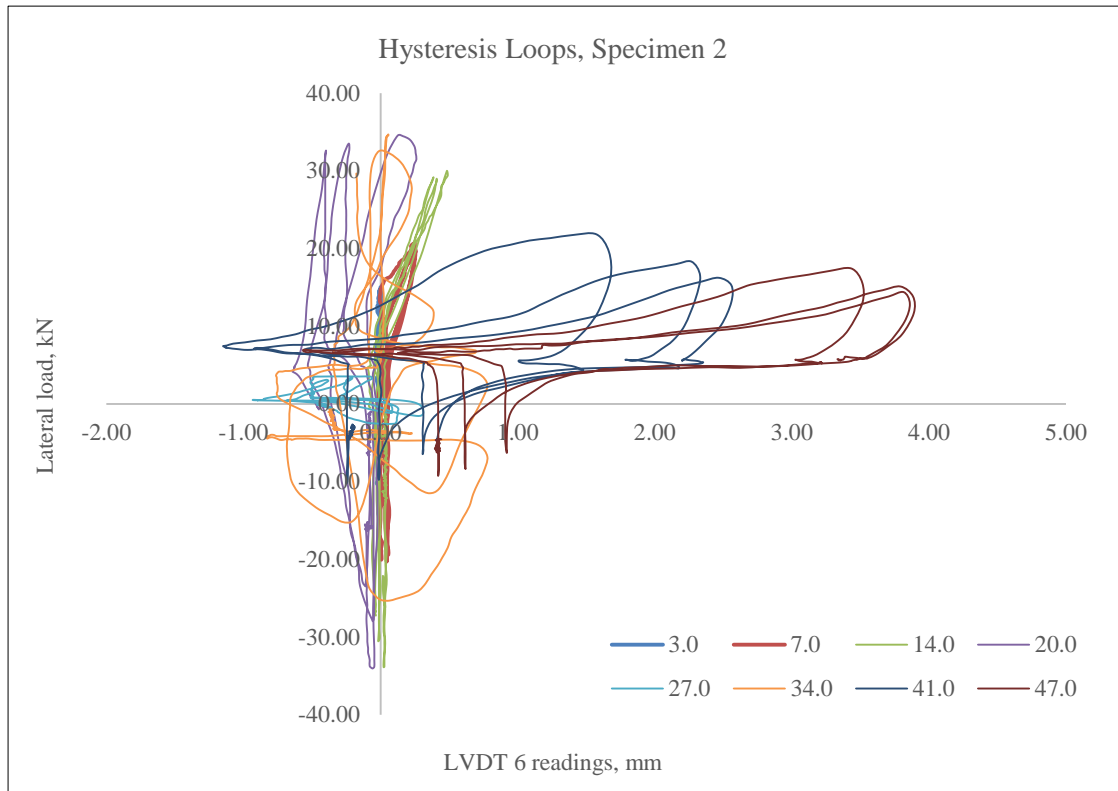
Figure 22. Beam bottom displacement at beam-column interface vs. lateral loads, Specimen 2

3.3. Joint Shear Deformation for Both Specimens

The joint shear deformation was calculated for both specimens as shown in Figure 23.

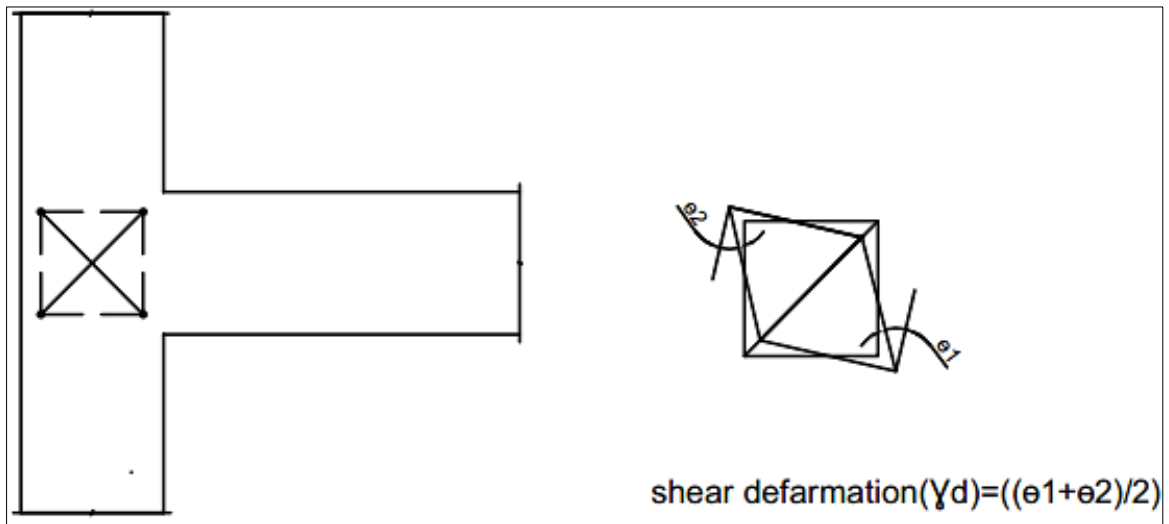shear deformation(γd)=((θ1+θ2)/2)

Figure 23. Joint shear deformation calculations

Joint shear deformations versus beam tip displacement for both specimens are shown in Figures 24 and 25. Specimen 1 showed no significant deformation as compared to specimen 2. Specimen 2 developed a maximum joint shear deformation of 0.014 radians while specimen 1 developed almost zero deformation. Due to high eccentricity in Specimen 2, torsional effect also added to the joint shear, produced extra demand on joint region. However, deformation in both specimens is negligible. This is primarily due to bond slip phenomenon in both specimens at joint regions due construction joint near beam longitudinal bars.
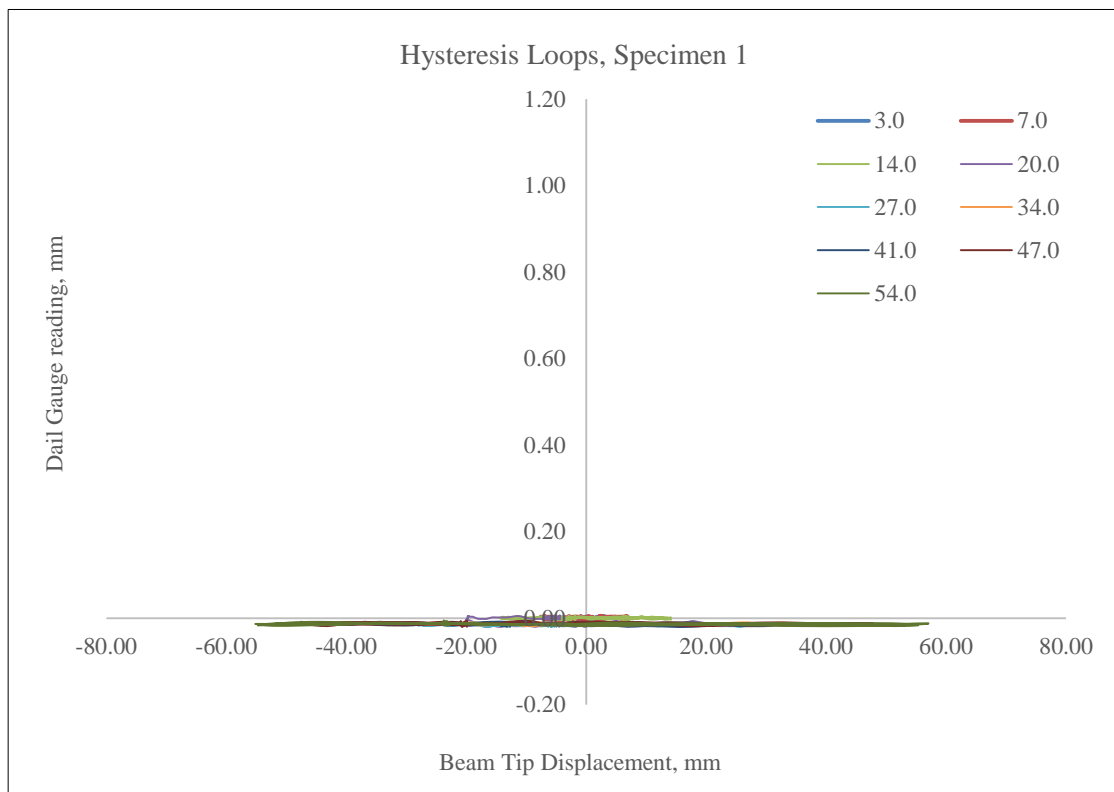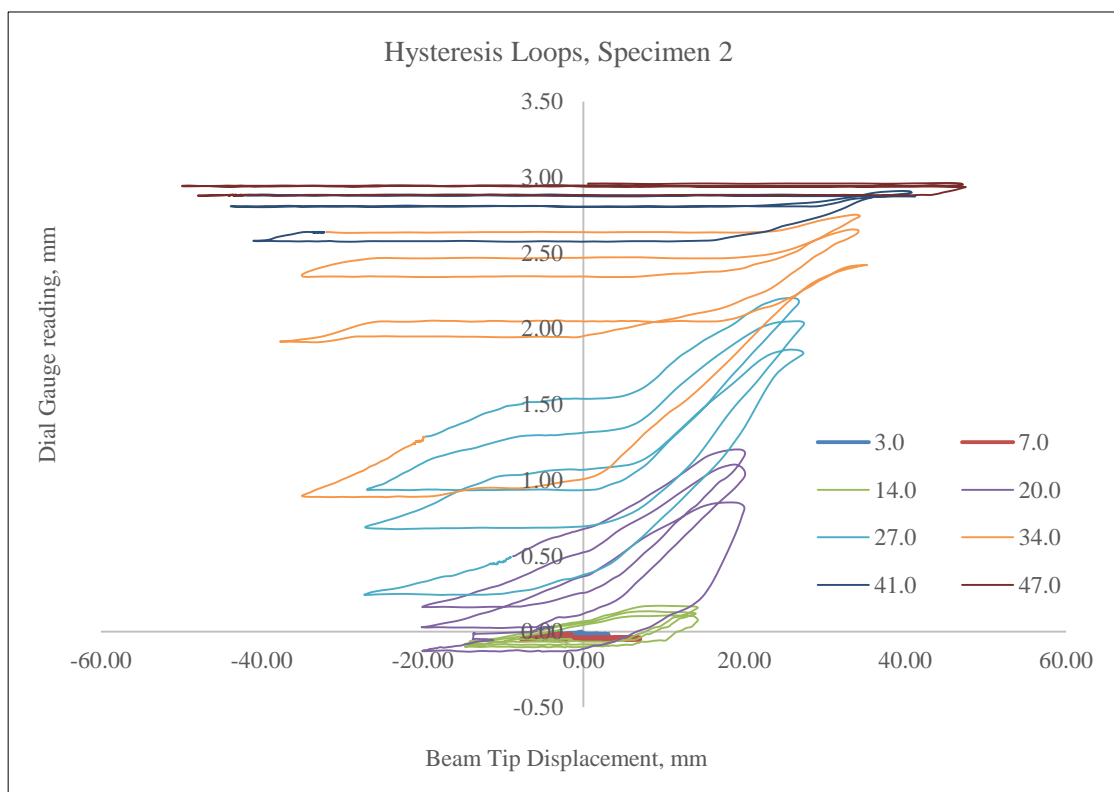
Figure 24. Joint shear deformation of specimen 1

Figure 25. Joint shear deformation of specimen 2

4. Conclusion

An experimental study was carried out to study the effect of eccentricity on performance of eccentric connections. A total of two specimens with different eccentricities were tested under quasi static cyclic loading. Both specimens consist of two columns (lower and upper parts) and two beams (spandrel and normal beam) along with slab. The main objective of this study was to study the damage pattern of the whole specimens, joint shear deformation and beam

rotation (in-plane and out of plane beam rotations). The principal failure pattern was observed to be bond slippage which occurred at 2.5% drift in both specimens with no yielding of beam longitudinal bars in the joint core due to the presence of construction joint and longer development length for longitudinal bars. The slippage was more in specimen 2 with greater eccentricity. An increase in out of plane rotation was observed with increase in eccentricity. However, in plane rotation was more in specimen 1 as compared to specimen 2 (58% greater), primarily due to negligible out of plane rotations. Furthermore, joint shear deformation increased with increase in eccentricity. However, it was negligible in both specimens due to slab contribution as well as bond slippage with minimum load transfer to the joint core.

5. Declarations

5.1. Data Availability Statement

The data presented in this study are available on request from the corresponding author.

5.2. Funding

5.3. Acknowledgements

5.4. Conflicts of Interest

The authors declare no conflict of interest.

6. References

[1] Joint ACI-ASCE Committee 352. Recommendations for Design of Beam-Column Connections in Monolithic Reinforced Concrete Structures (ACI 352R-02), American Concrete Institute, Farmington Hills, MI, 37 pp (2002).

[2] Shin, Myoungsu, and James M. LaFave. "Seismic performance of reinforced concrete eccentric beam-column connections with floor slabs." Structural Journal 101, no. 3 (2004): 403-412.

[3] Xing, G.H., T. Wu, D.T. Niu, and X. Liu. "Seismic Behavior of Reinforced Concrete Interior Beam-Column Joints with Beams of Different Depths." Earthquakes and Structures 4, no. 4 (April 25, 2013): 429–449. doi:10.12989/eas.2013.4.4.429.

[4] Raffaelle, Gregory S. "R/C eccentric beam-column connections subjected to earthquake-type loading." (1993): 5874-5874.

[5] Vollum, R. L., and J. B. Newman. "Towards the Design of Reinforced Concrete Eccentric Beam—column Joints." Magazine of Concrete Research 51, no. 6 (December 1999): 397–407. doi:10.1680/macr.1999.51.6.397.

[6] Hung-Jen, Lee, and Ko Jen-Wen. "Eccentric reinforced concrete beam-column connections subjected to cyclic loading in principal directions." ACI Structural Journal 104, no. 4 (2007): 459.

[7] Goto, Yasuaki, and Osamu Joh. "Shear resistance of RC interior eccentric beam-column joints." In 13th World Conference on Earthquake Engineering, (2004): 1-6.

[8] Li, Bing, Tso-Chien Pan, and Cao Thanh Tran. "Effects of Axial Compression Load and Eccentricity on Seismic Behavior of Nonseismically Detailed Interior Beam-Wide Column Joints." Journal of Structural Engineering 135, no. 7 (July 2009): 774–784. doi:10.1061/(asce)0733-9445(2009)135:7(774).

[9] Behnam, Hamdolah, J.S. Kuang, and Roy Y.C. Huang. "Exterior RC Wide Beam-Column Connections: Effect of Beam Width Ratio on Seismic Behaviour." Engineering Structures 147 (September 2017): 27–44. doi:10.1016/j.engstruct.2017.05.044.

[10] Di Franco, Marco A., Denis Mitchell, and Patrick Paultre. "Role of Spandrel Beams on Response of Slab-Beam-Column Connections." Journal of Structural Engineering 121, no. 3 (March 1995): 408–419. doi:10.1061/(asce)0733-9445(1995)121:3(408).

[11] Kim, Jaehong, and James M. LaFave. "Key Influence Parameters for the Joint Shear Behaviour of Reinforced Concrete (RC) Beam–column Connections." Engineering Structures 29, no. 10 (October 2007): 2523–2539. doi:10.1016/j.engstruct.2006.12.012.

[12] Joh, O., Y. Goto, and T. Shibata. "Behavior of reinforced concrete beam-column joints with eccentricity." Special Publication 123 (1991): 317-358.

[13] Canbolat, Burcu B., and James K. Wight. "Experimental investigation on seismic behavior of eccentric reinforced concrete beam-column-slab connections." ACI Structural Journal 105, no. 2 (2008): 154.

[14] ACI Committee 318, "Building Code Requirements for Structural Concrete (ACI 318-14)" American Concrete Institute, Farmington Hills, MI, (2014): 519.

[15] Lee, Hung-Jen, and Si-Ying Yu. "Cyclic response of exterior beam-column joints with different anchorage methods." ACI Structural Journal 106, no. 3 (2009): 329.

[16] Ma, Cailong, Zhenyu Wang, and Scott T. Smith. "Seismic Performance of Large-Scale RC Eccentric Corner Beam-Column-Slab Joints Strengthened with CFRP Systems." Journal of Composites for Construction 24, no. 2 (April 2020): 04019066. doi:10.1061/(asce)cc.1943-5614.0000995.

[17] Wong, Ho-Fai, Ying Liu, Sung-Hei Luk, Pok-Man Lee, and Wing-Hei Kwong. "Effects of eccentricity on seismic behavior of non-seismically designed reinforced concrete beam-column joint." (2019).

[18] Mogili, Srinivas, J. S. Kuang, and Roy Y. C. Huang. "Effects of Beam–column Geometry and Eccentricity on Seismic Behaviour of RC Beam–column Knee Joints." Bulletin of Earthquake Engineering 17, no. 5 (January 17, 2019): 2671–2686. doi:10.1007/s10518-019-00562-y.